Thermal properties of N-alkyl-N-methylpyrrolidinium and N-butylpyridinium fluorometallates and physicochemical properties of their melts

AUTHOR(S):

Kanatani, Takatsugu; Ueno, Ryuichi; Matsumoto, Kazuhiko; Nohira, Toshiyuki; Hagiwara, Rika

CITATION:

Kanatani, Takatsugu ...[et al]. Thermal properties of N-alkyl-N-methylpyrrolidinium and N-butylpyridinium fluorometallates and physicochemical properties of their melts. Journal of Fluorine Chemistry 2009, 130: 979-984

ISSUE DATE:

2009-10

URL:

http://hdl.handle.net/2433/261130

Thermal properties of *N*-alkyl-*N*-methylpyrrolidinium and *N*-butylpyridinium fluorometallates and physicochemical properties of their melts

Takatsugu Kanatani, Ryuichi Ueno, Kazuhiko Matsumoto, Toshiyuki Nohira, Rika Hagiwara*

Department of Fundamental Energy Science, Graduate School of Energy Science,

Kyoto University, Sakyo-ku, Kyoto 606-8501, Japan,

*E-mail: hagiwara@energy.kyoto-u.ac.jp

Tel: +81-75-753-5822

Fax: +81-75-753-5906

Key words**:** Pyrrolidinium, Ionic liquid, Fluorocomplex anion

Abstract

A series of *N*-alkyl-*N*-methylpyrrolidinium ($RMPyr^+$, where R = E: ethyl, B: butyl, and H: hexyl) and *N*-butylpyridinium (BPy^+) salts based on the fluorocomplex anions, BF_4^-, PF_6^-, SbF_6^-, NbF_6^-, TaF_6^-, and WF_7^- have been synthesized and their thermal behavior has been investigated. The melting points of the $RMPyr^+$ salts are above room temperature with the trend; $BMPyrAF_6$ < $HMPyrAF_6$ < $EMPyrAF_6$ for the hexafluorocomplex salts. Some of the salts containing $BMPyr^+$ and $HMPyr^+$ exhibit phase transitions in the solid states. Similar melting points of BPy^+ salts of PF_6^-, SbF_6^-, NbF_6^-, TaF_6^-, and WF_7^- are observed at around 350 K. Ionic conductivity and viscosity for $BMPyrNbF_6$ (3.0 mS cm^{-1} and 164 cP at 328 K) are similar to those for $BMPyrTaF_6$ (3.0 mS cm^{-1} and 165 cP at 328 K), resulting from the similarity of the anions in size. The activation energies of ionic conductivity for the NbF_6^- and TaF_6^- salts are 18 and 20 kJ mol^{-1}, and those for viscosity are 23 and 25 kJ mol^{-1}, respectively calculated by Arrhenius equation in the temperature range between 328 and 348 K. Electrochemical windows of $BMPyrNbF_6$, $BMPyrTaF_6$, and $BMPyrWF_7$ are about 4.0, 5.0 and 3.1 V, respectively.

1. Introduction

Ionic liquids (ILs) attract more and more attention in various fields, such as electrochemistry and organic chemistry, because of their unique properties such as low volatility, nonflammability, wide liquid-phase temperature ranges, and wide electrochemical windows [1-5]. Compared to the salts based-on the cations such as imidazolium and pyridinium, nonaromatic cation-based salts often exhibit high melting points and sometimes decompose without melting. On the other hand, the high electrochemical and chemical stabilities of the nonaromatic cation-based salts are large benefits in various applications including electric double layer capacitors (EDLC), fuel cells, lithium batteries, and solar cells [6-11]. Dialkylpyrrolidinium cations are nonaromatic, however, exceptionally give low temperature ionic liquids in the combination with selected anions such as fluorohydrogenate ($(FH)_nF^-$) and bis(trifluoromethylsulfonyl)amide ($TFSA^-$) anions [12, 13]. The pyrrolidinium cation-based salts also have received attention since they often form a plastic crystal phase [14-18] which are potential electrolytes in solar cells and Li-batteries [8].

Among the reported synthetic routes for ILs [19], fluoroacid-base reaction between fluorohydrogenate ILs and binary fluorides (AF_m) is one of the effective methods to reduce possible impurities such as water and chloride or bromide from raw materials. A series of 1-ethyl-3-methylimidazolium ($EMIm^+$) cation-based fluorocomplex salts of BF_4^-, PF_6^-, AsF_6^-, SbF_6^-, NbF_6^-, TaF_6^-, and WF_7^- were synthesized with this method and characterized by spectroscopic, physical, chemical, and electrochemical methods [20]. The melting points of the

series of the $EMIm^+$ salts decrease with increasing the size of the anion from the PF_6^- salt (333 K) to the WF_7^- salt (258 K) except for the BF_4^- salt (288 K).

In the present study, we report the syntheses of a series of *N*-alkyl-*N*-methylpyrrolidinium ($RMPyr^+$, where R = E: ethyl, B: butyl, and H: hexyl) and *N*-butylpyridinium (BPy^+) salts based on the fluorocomplex anions, BF_4^-, PF_6^-, SbF_6^-, NbF_6^-, TaF_6^-, and WF_7^- by fluoroacid-base reactions. Thermal behaviors of the obtained salts are also reported. The physical and electrochemical properties of the three salts with low melting temperatures, $BMPyrNbF_6$, $BMPyrTaF_6$, and $BMPyrWF_7$, are discussed in detail.

2. Results and discussion

2.1 Synthesis and vibrational spectroscopy

All the present fluorocomplex salts were prepared by the fluoroacid-base reactions of a fluorohydrogenate ionic liquid and the corresponding fluorides (Scheme 1) as previously reported [20] except SbF_6^- salts that were synthesized by the conventional ion exchange reactions of the corresponding chloride salts and $KSbF_6$ since the pyrrolidinium and pyridinium cations are not stable against the oxidation by SbF_5. For all the salts obtained above, the corresponding cation and anion were confirmed by vibrational spectroscopy, while only the spectroscopic features of $BMPyrNbF_6$, $BMPyrTaF_6$, and $BMPyrWF_7$ are briefly described here (see the Experimental section for the other salts).

Figures 1 and 2 show Raman and IR spectra, respectively, for $BMPyrNbF_6$, $BMPyrTaF_6$, and $BMPyrWF_7$. The vibrational modes of the BMPyr cation are observed at the expected positions in the spectra [14, 15]. For $BMPyrNbF_6$ and $BMPyrTaF_6$, the ν_3 mode of the anion is observed in the IR spectra at 615 and 561 cm^{-1}, respectively, and the ν_1 and ν_5 modes are observed in the Raman spectra (670 and 283 cm^{-1} for $BMPyrNbF_6$ and 683 and 287 cm^{-1} for $BMPyrTaF_6$) [21]. The Raman active ν_2 and IR active ν_4 mode are too weak to be detected in the present salts. Although the molecular geometry of WF_7^- in $BMPyrWF_7$ is unknown, the possible three candidates, monocapped octahedron, monocapped trigonal prism, and pentagonal bipyramid, are considered to give a strong peak at ~700 cm^{-1} in the Raman spectrum as reported in the previous literatures

[22-24]. The absorption band observed around 580 cm^{-1} in the IR spectrum also agrees with the band observed in other WF_7^- salts [20].

Thermal behaviors

The melting points and decomposition temperatures of a series of RMPyr and BPy salts are listed in Table 1. In the cases of EMPyr salts, the BF_4^- and PF_6^- salts exhibit melting points of 567 and 534 K, respectively, whereas the other salts of SbF_6^-, NbF_6^-, TaF_6^-, and WF_7^- decompose without melting. Although the melting point of $HMPyrBF_4$ is 345 K, the other $HMPyr^+$ salts of PF_6^-, SbF_6^-, NbF_6^-, TaF_6^-, and WF_7^- exhibit much higher melting points of around 450 K. The aromatic cation-based salts of BPy^+ based on PF_6^-, SbF_6^-, NbF_6^-, TaF_6^-, and WF_7^- exhibit melting points of around 350 K regardless of the anionic species. The pyrrolidinium cation-based salts, $HMPyrBF_4$ and $BMPyrAF_n$ (A = Sb, Nb, Ta (n = 6), W (n = 7)), exhibit several solid-solid transitions. Figure 3 and Table 2 show the DSC heating traces and phase transition temperature of $BMPyr^+$ salts of NbF_6^-, TaF_6^-, and WF_7^- anion, respectively. In the solid state, both NbF_6^- and TaF_6^- salts exhibit four solid phases. The broad exothermic peak observed for the NbF_6^- and TaF_6^- salts between the phases IV and III are assigned to the crystallization of a supercooled domain. On the other hand, the WF_7^- salt exhibits two solid phases assigned to the phase I and II, with a phase transition temperature of 202 K. The enthalpy and entropy changes of fusion, ΔH_f and ΔS_f, are also shown in Table 2. The ΔS_f value is calculated using the relationship $\Delta S_f = \Delta H_f / T_m$, where T_m is the melting point. Timmermans pointed out that plastic crystal phases typically

have an entropy change of fusion, lower than 20 J K^{-1} mol^{-1} [22]. This appears to be the cases for NbF_6^- of 7.6 J K^{-1} mol^{-1}, TaF_6^- of 10.1 J K^{-1} mol^{-1}, and WF_7^- salts of 12.7 J K^{-1} mol^{-1}, suggesting that the solid phase I for the present NbF_6^-, TaF_6^-, and WF_7^- salts is a plastic crystal phase [16, 17].

Figure 4 shows the melting points of the prepared salts as a function of the ionic radii of central atoms of the anions [12, 13]. The data for $EMImAF_m$ (A = P, As, Sb, Nb, Ta (m = 6), and W (m = 7)) [20] are also plotted for comparison. In the cases of $BMPyr^+$ salts, the melting point decreases with increase in size of the central atom, from 411 K for $BMPyrBF_4$ to 316 K for $BMPyrWF_7$. On the other hand, the melting points of $BPyPF_6$, $BPyNbF_6$, $BPyTaF_6$, and $BPyWF_7$ are not different significantly, 351, 357, 351, and 348 K, respectively. Comparing $BMPyr^+$ salts of NbF_6^-, TaF_6^-, and WF_7^- to the corresponding BPy^+ salts, $BMPyr^+$ salts exhibit melting points about 30 K lower than those of the BPy^+ salts. The melting points of these salts are determined by several factors, including lattice energy that is related to the crystal structure and interaction energy with the adjacent ions in the liquid state. The BF_4^- anion tends to show a lower melting point in spite of its small size, which is probably due to the different coordination environment around its tetrahedral shape from the larger hexa- or heptacoordinated anions. Further discussion requires the crystal structures and thermodynamic data for these compounds.

2.2 Physical and electrochemical properties

Table 3 lists ionic conductivity and viscosity for $BMPyrNbF_6$ and $BMPyrTaF_6$ in the

temperature range from 328 to 348 K. The ionic conductivity and viscosity of $BMPyrNbF_6$ are similar to those of $BMPyrTaF_6$. Figure 5 shows the Arrhenius plots of viscosity and conductivity for $BMPyrNbF_6$ and $BMPyrTaF_6$. The activation energies of ionic conductivity for the NbF_6^- and TaF_6^- salts are 18 and 20 kJ mol^{-1}, and those for viscosity are 23 and 25 kJ mol^{-1}, respectively calculated by Arrhenius equation in the temperature range between 328 and 348 K. The similarity in these values is considered to be the results of the similar size of the anions. Figure 6 shows the cyclic voltammograms of a glassy carbon electrode in $BMPyrNbF_6$, $BMPyrTaF_6$, and $BMPyrWF_7$ at 343 K. The cathode limits of NbF_6^-, TaF_6^-, and WF_7^- salts are -2.0, -2.8, and -0.8 V vs. Ag^+/Ag, respectively. These limits are assigned to the reductions of anions, because the reduction of $BMPyr^+$ is observed at around -3.0 V vs. Ag^+/Ag [17, 27]. Although the reactions at the cathode limits for the three $BMPyr^+$ salts are unknown, the difference of the reduction potential is due to the difference in stability of the anion against reduction, which is supported by the similar reduction potentials to the cases of the $EMIm^+$ salts of NbF_6^-, TaF_6^-, and WF_7^- (-2.0, -2.9, and -0.8 V vs. Ag^+/Ag, respectively) [20]. On the other hand, the anode limits of NbF_6^-, TaF_6^-, and WF_7^- were +2.0, +2.2, and +2.3 V vs. Ag^+/Ag, respectively, and assigned to the oxidations of $BMPyr^+$. In conclusion, the electrochemical windows of $BMPyrNbF_6$, $BMPyrTaF_6$, and $BMPyrWF_7$ are 4.0, 5.0 and 3.1 V, respectively.

3. Experimental

3.1 General experimental procedure

Moisture sensitive materials were handled in a glove box under a dry Ar atmosphere. All the reactions involved with anhydrous HF (aHF, Daikin Industries, purity > 99 %) were performed in PFA reactors. Anhydrous HF was dried over K_2NiF_6 (Ozark-Mahoning) for several days prior to use. The starting chlorides, RMPyrCl and BPyCl, were prepared by the reactions of the corresponding amine and chloroalkane. The fluorohydrogenate salts were prepared by the reactions of the chloride and a large excess of aHF. Volatile materials were pumped off at room temperature after the reaction. Boron trifluoride (Nippon Sanso, purity 99.99%), PF_5 (Nippon Sanso, purity 99%), antimony pentafluoride (SbF_5, PCR, purity > 97%), $KSbF_6$ (Aldrich, purity 99 %), NbF_5 (Aldrich, purity 99 %), TaF_6 (Aldrich, purity 99.5 %), and WF_6 (Central Glass, purity 99.999 %) were used as supplied.

3.2 Spectroscopic measurement

Raman spectra of solid and liquid samples were obtained by LabRAM300 (Horiba Jobin Yvon) using 632 nm line of He-Ne laser as an excitation line at room temperature. The samples for Raman spectroscopy were loaded in NMR Pyrex test tubes. The IR spectra of solid and liquid samples were obtained by FTS-165 (BIO-RAD Laboratories). The samples were sandwiched by a pair of AgCl windows fixed in a stainless airtight cell.

3.3 Measurement of physical and electrochemical properties

Differential scanning calorimetric analysis (DSC) was performed on the sample in an aluminium sealed cell under dry Ar gas flow using a Shimadzu DSC-60. The scanning rate of 10 K min^{-1} was used. Conductivity and electrochemical window were measured by AC impedance spectroscopy and cyclic voltammetry, respectively, with the aid of HZ-3000 electrochemical measurement system (Hokuto Denko). The cell for conductivity measurement was made of PFA and PTFE (polytetrafluoroethylene) with platinum disk electrodes and was calibrated by a KCl standard aqueous solution. The working and counter electrodes for electrochemical window measurement were glassy carbon, on the other side, reference electrode was Ag wire immersed in $EMIMBF_4$ containing 0.05 M $AgBF_4$. Viscosity was measured by a cone-plate rheometer DV-II + Pro (Brookfield Engineering Laboratories Inc.).

3.4 Synthesis

3.4.1. Synthesis of $EMPyrBF_4$

Boron trifluoride was condensed on $EMPyr(FH)_{2.3}F$ (5.58 mmol) at 77 K in a PFA tube. After warming up to room temperature, the mixture was mixed well. This procedure was repeated several times until the reaction finishes. A colorless solid was obtained after the removal of liberated HF and excess BF_3 under dynamic vacuum at 300 K. Anal. Calcd. for $C_7F_4H_{16}N_1B_1$: C, 41.83; H, 8.02; N, 6.97. Found: C, 41.79; H, 7.94; N, 6.99. Raman (frequency/ cm^{-1} (Relative intensity)): 739(s) (BF_4^-, ν_1). IR (frequency/ cm^{-1} (Relative intensity)): 1049 (s) (BF_4^-, ν_3), 524(s) (BF_4^-, ν_4). Here, s and w for relative intensity denote strong and weak, respectively.

3.4.2 Synthesis of $EMPyrPF_6$

The same procedure as for $EMPyrBF_4$ was used. Anal. Calcd. for $C_7F_6H_{16}N_1P_1$: C, 32.44; H, 6.22; N, 5.40. Found: C, 32.16; H, 5.94; N, 5.41. Raman (frequency/ cm^{-1} (Relative intensity)): 738(s) (PF_6^-, ν_1). IR (frequency/ cm^{-1} (Relative intensity)): 845(s) (PF_6^- ν_3), 559(s) (PF_6^-, ν_4).

3.4.3 Synthesis of $EMPyrSbF_6$

EMPyrCl (5.58 mmol) and equivalent $KSbF_6$ (5.56 mmol) were reacted in acetone, and most amount of byproduct KCl was eliminated by filtration. After removing acetone, water and dichloroethane were added to the $EMPyrSbF_6$ and KCl mixture for extraction. A white powder of $BMPyrSbF_6$ was obtained by removing water containing KCl, and dichlooroethane under dynamic vacuum at 300 K. Anal. Calcd. for $C_7F_6H_{16}N_1Sb_1$: C, 24.02; F, 32.57; H, 4.61; N, 4.00. Found: C, 23.54; F, 32.08; H, 4.43; N, 3.91. Raman (frequency/ cm^{-1} (Relative intensity)): 645(s) (SbF_6^-, ν_1), 278(w) (SbF_6^-, ν_5). IR (frequency/ cm^{-1} (Relative intensity)): 663(s) (SbF_6^-, ν_3).

3.4.4 Synthesis of $EMPyrNbF_6$

$EMPyr(FH)_{2.3}F$ (4.82 mmol) and equimolar NbF_5 (4.82 mmol) were reacted in a T-shaped PFA reactor. A colorless powder sample was obtained after the removal of liberated HF under dynamic vacuum at 340 K. Raman and IR spectroscopy and elemental analyses identified the solid was $BMPyrNbF_6$. Anal. Calcd. for $C_7F_6H_{16}N_1Nb_1$: C, 26.18; F, 35.50; H, 5.02; N, 4.36. Found: C, 25.55; F, 35.11; H, 4.77; N, 4.30. Raman (frequency/ cm^{-1} (Relative intensity)): 676(s) (NbF_6^-, ν_1), 278(w) (NbF_6^-, ν_5). IR (frequency/ cm^{-1} (Relative intensity)): 617(s) (NbF_6^-, ν_3).

3.4.5 Synthesis of EMPyrTaF$_6$

The same procedure as for EMPyrNbF$_6$ was used. Anal. Calcd. for $C_7F_6H_{16}N_1Ta_1$: C, 20.55; F, 27.86; H, 3.94; N, 3.42. Found: C, 20.00; F, 27.05; H, 3.72; N, 3.38. Raman (frequency/ cm^{-1} (Relative intensity)): 691(s) (TaF_6^-, ν_1), 282(w) (TaF_6^-, ν_5). IR (frequency/ cm^{-1} (Relative intensity)): 578(s) (TaF_6^-, ν_3).

3.4.6 Synthesis of EMPyrWF$_7$

The same procedure as for EMPyrBF$_4$ was used. Anal. Calcd. for $C_7F_7H_{16}N_1W_1$: C, 19.51; F, 30.85; H, 3.74; N, 3.25. Found: C, 20.98; F, 23.00; H, 4.22; N, 3.51. Raman (frequency/ cm^{-1} (Relative intensity)): 629(s) (WF_7^-). IR (frequency/ cm^{-1} (Relative intensity)): 615(s) (WF_7^-).

3.4.7 Synthesis of BMPyrSbF$_6$

The same procedure as for EMPyrSbF$_6$ was used. Anal. Calcd. for $C_7F_6H_{16}N_1Sb_1$: C, 28.60; F, 30.16; H, 5.33; N, 3.71. Found: C, 28.65; F, 29.62; H, 5.32; N, 3.77. Raman (frequency/ cm^{-1} (Relative intensity)): 645(s) (SbF_6^-, ν_1), 570(vw) (SbF_6^-, ν_2), 279 (m) (SbF_6^-, ν_5). IR (frequency/ cm^{-1} (Relative intensity)): 653(s) (SbF_6^-, ν_3). Here, m and vw for relative intensity denote medium and very weak, respectively.

3.4.8 Synthesis of BMPyrNbF$_6$

The same procedure as for EMPyrNbF$_6$ was used. Anal. Calcd. for $C_9F_6H_{20}N_1Nb_1$: C, 30.96; F, 32.65; H, 5.77; N, 4.01. Found: C, 30.69; F, 32.55; H, 5.60; N, 4.02. Raman (frequency/ cm^{-1} (Relative intensity)): 670(s) (NbF_6^-, ν_1), 283(w) (NbF_6^-, ν_5). IR (frequency/ cm^{-1} (Relative

intensity)): 615(s) (NbF_6^-, ν_3).

3.4.9 Synthesis of BMPyrTaF$_6$

The same procedure as for EMPyrNbF$_6$ was used. Anal. Calcd. for $C_9F_6H_{20}N_1Ta_1$: C, 24.73; F, 26.07; H, 4.61; N, 3.20. Found: C, 25.85; F, 25.30; H, 4.68; N, 3.47. Raman (frequency/ cm^{-1} (relative intensity)): 683(s) (TaF_6^-, ν_1), 290(w) (TaF_6^-, ν_5). IR (frequency/ cm^{-1} (relative intensity)): 586(s) (TaF_6^-, ν_3).

3.4.10 Synthesis of BMPyrWF$_7$

The same procedure as for EMPyrBF$_4$ was used. Anal. Calcd. for $C_9F_7H_{20}N_1W_1$: C, 23.55; F, 28.97; H, 4.39; N, 3.05. Found: C, 24.00; F, 26.80; H, 4.48; N, 3.16. Raman (frequency/ cm^{-1} (Relative intensity)): 700(s), 307(w) (WF_7^-). IR (frequency/ cm^{-1} (Relative intensity)): 619(s) (WF_7^-).

3.4.11 Synthesis of HMPyrBF$_4$

The same procedure as for EMPyrBF$_4$ was used. Anal. Calcd. for $C_{11}F_4H_{24}N_1B_1$: C, 51.38; H 9.41; N, 5.45. Found: C, 49.47; H 9.09; N, 5.26. Raman (frequency/ cm^{-1} (Relative intensity)): 764(s) (BF_4^-, ν_1). IR (frequency/ cm^{-1} (Relative intensity)): 1072(s) (BF_4^-, ν_3), 524(w) (BF_4^-, ν_4).

3.4.12 Synthesis of HMPyrPF$_6$

The same procedure as for EMPyrBF$_4$ was used. Anal. Calcd. for $C_{11}F_6H_{24}N_1P_1$: C, 41.9; H, 7.67; N, 4.44. Found: C, 41.94; H, 7.72; N, 4.40. Raman (frequency/ cm^{-1} (Relative intensity)): 738(s) (PF_6^-, ν_1). IR (frequency/ cm^{-1} (Relative intensity)): 849(s) (PF_6^-, ν_3), 559(s) (PF_6^-, ν_4).

3.4.13 Synthesis of HMPyrSbF$_6$

The same procedure as for EMPyrSbF$_6$ was used. Anal. Calcd. for $C_{11}F_6H_{24}N_1Sb_1$: C, 32.54; F, 28.07; H, 5.96; N, 3.45. Found: C, 30.48; F, 28.2; H, 5.53; N, 3.29. Raman (frequency/ cm^{-1} (Relative intensity)): 644(s) (SbF_6^-, ν_1), 278(w) (SbF_6^-, ν_5). IR (frequency/ cm^{-1} (Relative intensity)): 659(s) (SbF_6^-, ν_3).

3.4.14 Synthesis of HMPyrNbF$_6$

The same procedure as for EMPyrSbF$_6$ was used. Anal. Calcd. for $C_{11}F_6H_{24}N_1Nb_1$: C, 35.02; F, 30.22; H, 6.41; N, 3.71. Found: C, 34.77; F, 28.74; H, 6.35; N, 3.70. Raman (frequency/ cm^{-1} (Relative intensity)): 677(s) (NbF_6^-, ν_1), 274(w) (NbF_6^-, ν_5). IR (frequency/ cm^{-1} (Relative intensity)): 774(s) (NbF_6^-, ν_3).

3.4.15 Synthesis of HMPyrTaF$_6$

The same procedure as for EMPyNbF$_6$ was used. Anal. Calcd. for C11F6H24N1Ta1: C, 28.4; F, 24.5; H, 5.20; N, 3.01. Found: C, 29.37; F, 24.4; H, 5.27; N, 3.09. Raman (frequency/ cm^{-1} (Relative intensity)): 687(s) (TaF_6^-, ν_1), 282(w) (TaF_6^-, ν_5). IR (frequency/ cm^{-1} (Relative intensity)): 598(s) (TaF_6^-, ν_3).

3.4.16 Synthesis of HMPyrWF$_7$

The same procedure as for EMPyrBF$_4$ was used. Anal. Calcd. for $C_{11}F_7H_{24}N_1W_1$: C, 27.12; F, 27.30; H, 4.97; N, 2.88. Found: C, 28.17; F, 20.61; H, 5.33; N, 3.04. Raman (frequency/ cm^{-1} (Relative intensity)): 703(s) (WF_7^-). IR (frequency/ cm^{-1} (Relative intensity)): 632(s) (WF_7^-).

3.4.17 Synthesis of $BPyPF_6$

The same procedure as for $EMPyrBF_4$ was used. Anal. Calcd. for $C_7F_6H_{16}N_1P_1$: C, 38.44; H, 5.02; N, 4.98. Found: C, 38.32; H, 4.80; N, 4.99. Raman (frequency/ cm^{-1} (Relative intensity)): 728(s) (PF_6^-, ν_1). IR (frequency/ cm^{-1} (Relative intensity)): 839(s) (PF_6^-, ν_3), 549 (PF_6^-, ν_4).

3.4.18 Synthesis of $BPySbF_6$

The same procedure as for $EMPyrSbF_6$ was used. Anal. Calcd. for $C_7F_6H_{16}N_1Sb_1$: C, 29.06; F, 30.65; H, 3.79; N, 3.77. Found: C, 28.86; F, 30.15; H, 3.71; N, 3.76. Raman (frequency/ cm^{-1} (Relative intensity)): 643(s) (SbF_6^-, ν_1), 581(w) (SbF_6^-, ν_2), 284(m) (SbF_6^-, ν_5). IR (frequency/ cm^{-1} (Relative intensity)): 645(s) (SbF_6^-, ν_3).

3.4.19 Synthesis of $BPyNbF_6$

The same procedure as for $EMPyrNbF_6$ was used. Anal. Calcd. for $C_7F_6H_{16}N_1Nb_1$: C, 31.51; F, 33.22; H, 4.11; N, 4.08. Found: C, 32.02; F, 33.10; H 4.04; N, 4.19. Raman (frequency/ cm^{-1} (Relative intensity)): 687(s) (NbF_6^-, ν_1), 287(w) (NbF_6^-, ν_5). IR (frequency/ cm^{-1} (Relative intensity)): 608(s) (NbF_6^-, ν_3).

3.4.20 Synthesis of $BPyTaF_6$

The same procedure as for $EMPyrNbF_6$ was used. Anal. Calcd. for $C_7F_6H_{16}N_1Ta_1$: C, 25.07; F, 26.44; H, 3.27; N, 3.25. Found: C, 25.11; F, 26.31; H 3.09; N, 3.20. Raman (frequency/ cm^{-1} (Relative intensity)): 687(s) (TaF_6^-, ν_1), 292(w) (TaF_6^-, ν_5). IR (frequency/ cm^{-1} (Relative intensity)): 570(s) (TaF_6^-, ν_3).

3.4.21 Synthesis of $BPyWF_7$

The same procedure as for $EMPyrBF_4$ was used. Anal. Calcd. for $C_7F_7H_{16}N_1W_1$: C, 23.86; F, 29.35; H 3.11; N, 3.09. Found: C, 24.97; F, 22.69; H 3.34; N, 3.23. Raman (frequency/ cm^{-1} (Relative intensity)): 705(s) (WF_7^-). IR (frequency/ cm^{-1} (Relative intensity)): 619(s) (WF_7^-).

Acknowledgement

This research was supported by Grant-In-Aid for Scientific Research for Priority Areas, Science of Ionic Liquids, by Ministry of Education, Culture, Sports, Science and Technology.

References

1. T. Welton, Chem. Rev. 99 (1999) 2071-2083.
2. R. Hagiwara, Y. Ito, J. Fluorine Chem. 105 (2000) 221-227.
3. K. R. Seddon, J Chem. Technol. Biotechnol. 68 (1997) 351-356.
4. J. Fuller, R. T. Carlin, and R. A. Osteryoung, J. Electrochem. Soc. 144 (1997) 3881-3886.
5. P. Wasserscheid, W. Keim, Angew. Chem. Int. Ed. 39 (2000) 3772-3789.
6. M. Galiński, A. Lewandowski, I. Stępniak, Electrochim. Acta. 51 (2006) 5567–5580.
7. D.R. MacFarlane, J. Huang and M. Forsyth, Nature 402 (1999) 792-794.
8. N. Papageorgiou, Y. Athanassov, M. Armand, P. Bonhôte, H. Pettersson, A. Azam,b?? and M. Grätzel, J. Electrochem. Soc. 143 (1996) 3099-3108.

9. H. Ye, J. Huanga, J.J. Xua, N.K.A.C. Kodiweera, J.R.P. Jayakody, S.G. Greenbaum, J. Power Sources, 178 (2008) 651-660.

10. T. Sato, G. Masuda, Electrochimica Acta, 49 (2004) 3603-3611.

11. T. Sugimoto, Y. Atsumi, M. Kikuta, E. Ishiko, M. Kono, M. Isikawa, J. Power Sources 189 (2009) 802-805.

12. J. Sun, M. Forsyth, D. R. MacFarlane, J. Phys. Chem. B 102 (1998) 8858–8864.

13. K. Matsumoto, R. Hagiwara, Y. Ito, Electrochem. Solid-State Lett. 7 (2004) E41-E44.

14. J. Goldman, N. Hamid. D. R. MacFarlane, M. Forsyth, C. Forsyth, C. CoLLins, J. Huang, Chem. Mater. 13 (2001) 558-564.

15. S. Forsyth, J. Golding, D. R. MacFarlane, M. Forsyth, Electrochim. Acta. 46 (2001) 1753–1757.

16. W. A. Henderson, V. G. Young, Jr., S. Passerini, P. C. Trulove, and H. C. De Long, Chem. Mater. 18 (2006) 934-938.

17. D. R. MacFarlane, P. Meakin, J. Sun, N. Amini, M. Forsyth J. Phys. Chem. B 103 (1999) 4164–4170.

18. Leslie Glasser, Thermochim. Acta. 421 (2004) 87-93.

19. H. Xue, R. Verma, J.M. Shreeve, J. Fluorine Chem. 127 (2006) 159-176.

20. K. Matsumoto, R. Hagiwara, R. Yoshida, Y. Ito, Z. Mazej, P. Benkič, B. Žemva, O. Tamada, H. Yoshino, S. Matsubara, Dalton Trans. (2004) 144-149.

21. K. Nakamoto, Infrared and Raman Spectra of Inorganic and Coordination Compounds. Part A.Theory and Application in Inorganic Chemistry, Wiley Interscience, New York, 5th edn., 1997, p. 217.

22. A. Beuter, W. Kuhlmann, W. Sawodny, J. Fluorine Chem. 6 (1975) 367-378.

23. S. Giese, K. Seppelt, Angew. Chem. Int. Ed. Engl. 33 (1994) 461-463.

24. L. Arnaudet, R. Bougon, B. Ban, M. Lance, A. Navaza, M. Neirlich, J. Vigner, J. Fluorine Chem. 67 (1994) 14-25.

25. J. Timmermans, J. Phys. Chem. Solids 18 (1961) 1-8.

26. R. D. Shannon, Acta Cryst. A32 (1976) 751-767.

27. H. Sakaebe, H. Matsumoto, Electrochem. Commun. 5 (2003) 594-598.

Table 1 Melting points and decomposition temperatures of RMPyr and BPy fluorocomplex salts

		M.W.	T_m / K	T_d / K
EMPyr	BF_4	201	567	697
	PF_6	259	534	657
	SbF_6	350	–	651
	NbF_6	321	–	663
	TaF_6	409	–	670
	WF_7	431	–	659
BMPyr	SbF_6	378	326	633
	NbF_6	349	320	639
	TaF_6	437	323	637
	WF_7	459	322	635
HMPyr	BF_4	259	345	613
	PF_6	315	467	608
	SbF_6	406	453	623
	NbF_6	377	439	623
	TaF_6	465	448	673
	WF_7	487	456	710
BPy	PF_6	281	351	518
	SbF_6	371	351	603
	NbF_6	343	357	573
	TaF_6	431	351	633
	WF_7	453	348	603

M.W.: molecular weight, T_m: melting point, T_d: decomposition temperature

Table 2 Summary of thermal transition temperatures for BMPyr salts

	$T_{IV\rightarrow III}$ / K	$T_{III\rightarrow II}$ / K	$T_{II\rightarrow I}$ / K	T_m. / K	ΔH_f (kJ mol^{-1})	ΔS_f (J K^{-1} mol^{-1})
$BMPyrNbF_6$	195	278	305	320	2.44	7.6
$BMPyrTaF_6$	198	273	303	323	3.27	10.1
$BMPyrWF_7$	–	–	202	322	4.09	12.7

T_m: Melting temperature, ΔH_f: Enthalpy change of fusion, ΔS_f: Entropy change of fusion

Table 3 Summary of ionic conductivity and viscosity of $BMPyrNbF_6$ and $BMPyrTaF_6$ in the temperature range of 328 K to 348 K

Temperature/ K		328	333	338	343	348
$BMPyrNbF_6$	η / cP	164	126	106	87	74
	σ / mS cm^{-1}	3.0	3.5	4.2	4.8	5.5
$BMPyrTaF_6$	η / cP	165	128	110	89	70
	σ / mS cm^{-1}	3.0	3.5	4.2	5.1	5.8

η: viscosity, σ: ionic conductivity

Scheme and figure captions

Scheme 1 Preparation of the fluorocomplex salts and the structures of the cations used in the current study.

Figure 1 IR spectra of (a) BMPyrCl, (b) $BMPyrNbF_6$, (c) $BMPyrTaF_6$, and (d) $BMPyrWF_7$.

Figure 2 Raman spectra of (a) BMPyrCl, (b) $BMPyrNbF_6$, (c) $BMPyrTaF_6$, and (d) $BMPyrWF_7$.

Figure 3 DSC curves for (a) $BMPyrNbF_6$, (b) $BMPyrTaF_6$, and (c) $BMPyrWF_7$.

Figure 4 Relationship between the melting point and radius of the central atom of the anion for the fluorocomplex salts: (a) EMPyr, (b) BMPyr, (c) HMPyr, (d) BPy, and (e) EMIm.

Figure 5 Temperature dependency of viscosity and ionic conductivity for $BMPyrNbF_6$ and $BMPyrTaF_6$ in the temperature range of 325 to 353K.

Figure 6 Cyclic voltammograms of a glassy carbon electrode in (a) $BMPyrNbF_6$, (b) $BMPyrTaF_6$, and $BMPyrWF_7$.

Scheme 1

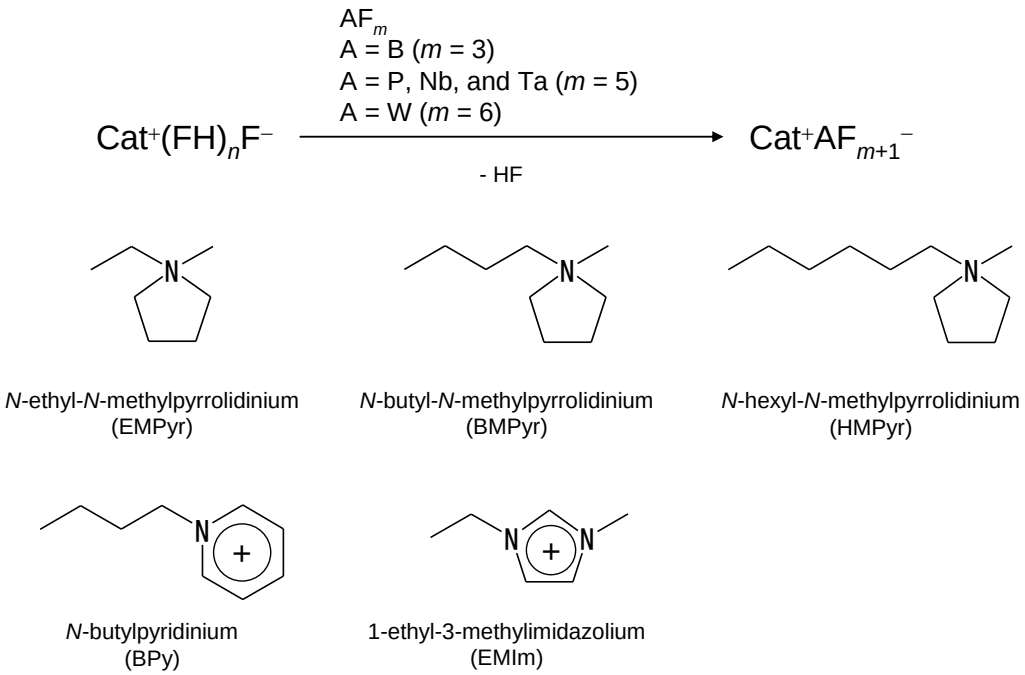

Figure 1

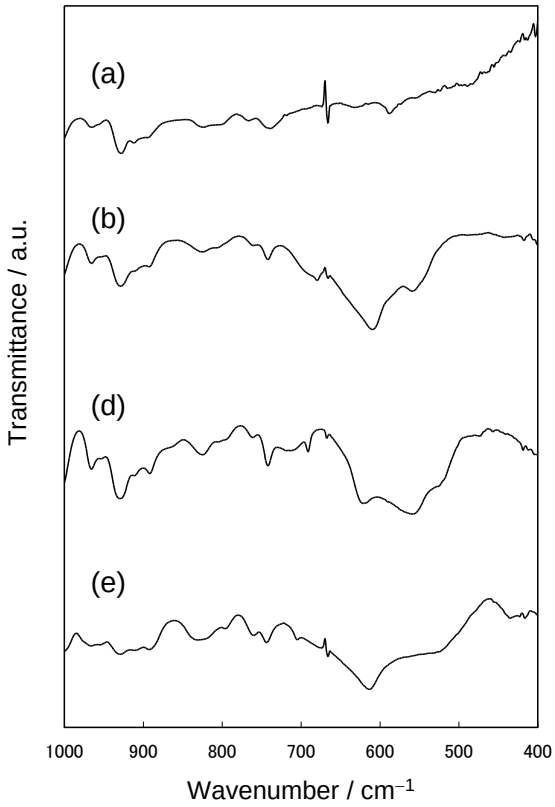

Figure 2

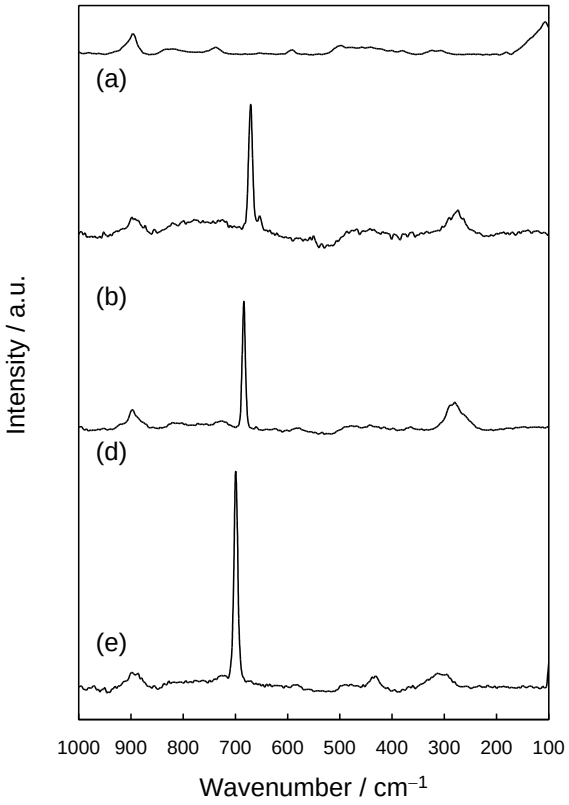

Figure 3

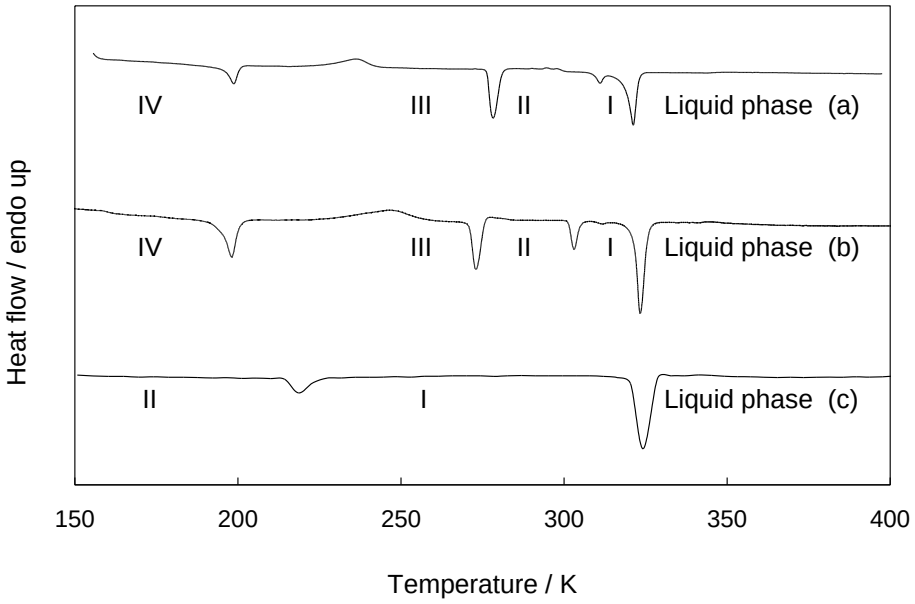

Figure 4

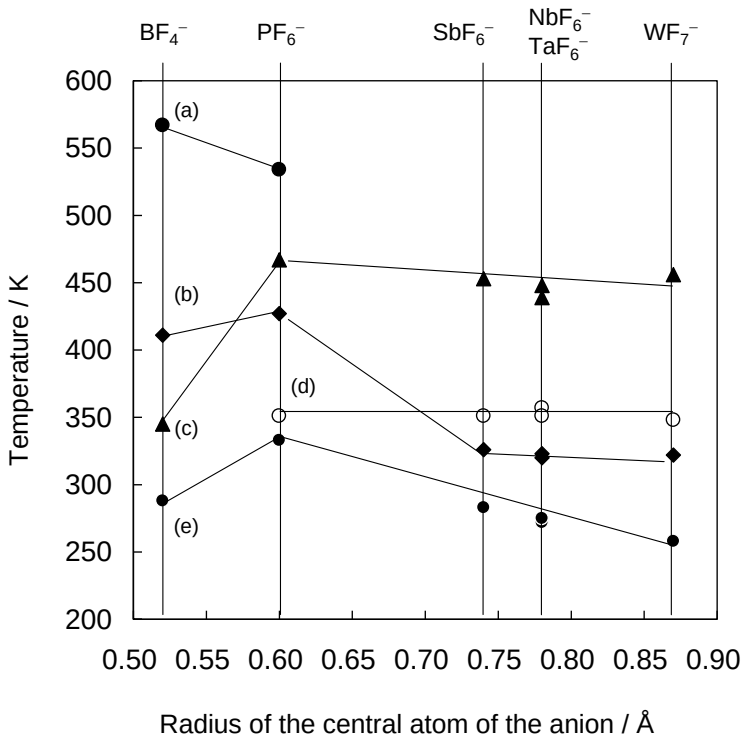

Figure 5

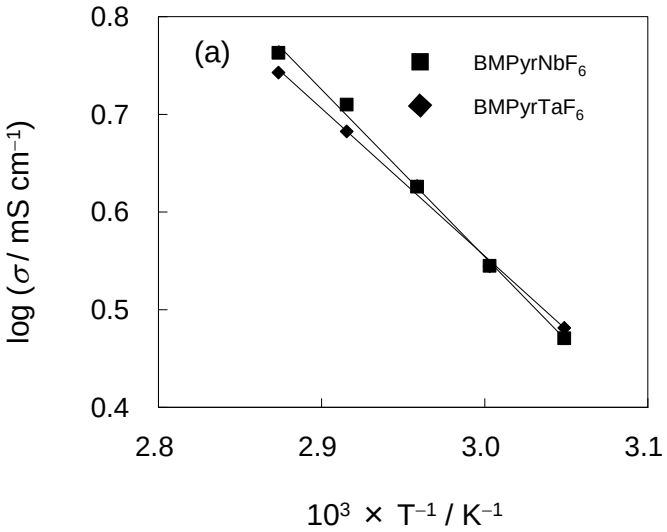

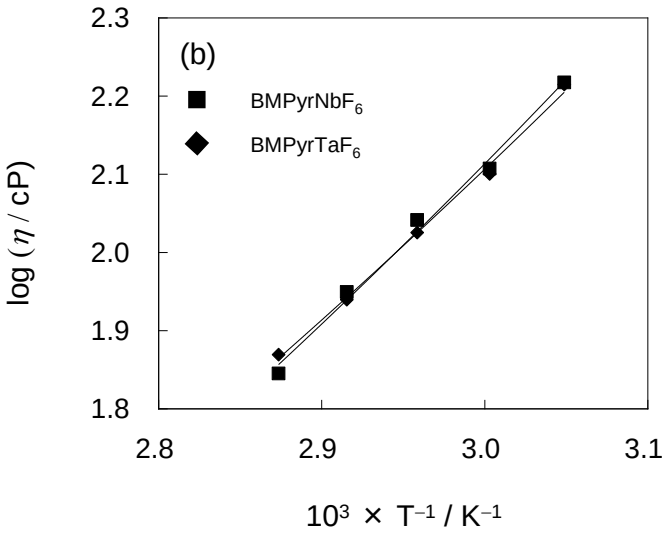

Figure 6